Available online at www.sciencedirect.com

SCIENCE DIRECT®

Coastal Engineering 52 (2005) 237–256

Coastal Engineering
An International Journal for Coastal, Harbour and Offshore Engineers

www.elsevier.com/locate/coastaleng

On convergence behaviour and numerical accuracy in stationary SWAN simulations of nearshore wind wave spectra

Marcel Zijlema[a,b,*], André J. van der Westhuysen[a]

[a]*Environmental Fluid Mechanics Section, Faculty of Civil Engineering and Geosciences, Delft University of Technology, P.O. Box 5048, 2600 GA Delft, The Netherlands*

[b]*National Institute for Coastal and Marine Management/RIKZ, P.O. Box 20907, 2500 EX The Hague, The Netherlands*

Received 9 December 2003; received in revised form 1 July 2004; accepted 9 December 2004

Abstract

Irregular convergence behaviour is frequently encountered when computations of wave spectra are performed by means of the third-generation wind wave model SWAN (Simulating WAve Nearshore). Numerical accuracy is another key issue. The present paper proposes two techniques that improve the convergence and accuracy properties of SWAN in the prediction of stationary wave conditions in the nearshore zone. The first is an under-relaxation approach in which the extent of updates during the iteration process, which underlies a route to steady state, is made proportional to wave frequency. This method complies with the principle of decreasing time scales at higher frequencies, which is inherent to the evolution of wind waves. As a result, the improved SWAN model is free from numerical restrictions to spectral shape in the non-equilibrium range. The second proposed method is a new termination criterion associated with the rate of model convergence, by which the identification of the point of convergence is improved. The capabilities of these methods are demonstrated by simulations of idealized cases and a field application featuring fetch- and depth-limited wave growth. It is concluded that the proposed termination criterion improves numerical accuracy and that the action density limiter, as currently used in SWAN, has minimal negative influence on stationary model results.

Keywords: Stationary wind wave spectra; Convergence behaviour; Numerical accuracy; Limiter; Frequency-dependent under-relaxation; Stopping criteria

1. Introduction

The search for reliable wave estimates for assessing the impact of waves on the natural environment, coastal protection, ship routing, offshore structures and port and harbour operations has led, over the past two decades, to the development of advanced spectral

* Corresponding author. Environmental Fluid Mechanics Section, Faculty of Civil Engineering and Geosciences, Delft University of Technology, P.O. Box 5048, 2600 GA Delft, The Netherlands. Tel.: +31 15 278 3255; fax: +31 15 278 4842.

E-mail address: m.zijlema@citg.tudelft.nl (M. Zijlema).

0378-3839/$ - see front matter © 2005 Elsevier B.V. All rights reserved.
doi:10.1016/j.coastaleng.2004.12.006

wind wave models known as third-generation models, such as WAM (WAMDI Group, 1988; Komen et al.,1994), WAVEWATCH III (Tolman, 1991) and SWAN (Booij et al., 1999). These models solve the spectral action balance equation without any a priori restrictions on the evolving spectrum during wave growth. To this end, the processes of generation by wind, dissipation by whitecapping and nonlinear wave–wave interactions have been explicitly parameterized. Whereas the models WAM and WAVEWATCH III consider non-stationary problems on oceanic scales, with SWAN wave propagation is usually calculated from deep water to the surf zone by means of solving the time-independent wave action balance equation. This is considered to be acceptable, since the residence time of the waves in the coastal zone is expected to be far less than the time scale of variations of the ambient current, the wind or the tide (Booij et al., 1999).

The accuracy with which physical processes for wave growth are approximated numerically is of crucial importance in assessing the predictive realism of spectral wave models. There is a need to separate these numerical errors from errors due to physical modelling. Third-generation wave models pose a numerical difficulty caused by the presence of multiple time scales. This is a reflection of the physical nature of wind waves, which consist of a wide range of frequencies. The ratio of the largest to the smallest time scale of spectral components is often substantially larger than one. When this is the case, the action balance equation is called stiff (Press et al., 1993)[1]. Taking proper account of these time scales is a necessary condition for numerical accuracy. This would require the use of a very small time step in a numerical algorithm, which may be impractical. Moreover, the action balance equation is usually so stiff that its numerical implementation combined with economically large time steps often prevent a stable solution. In this respect, nonlinear four-wave interaction usually poses the biggest problem, since this process is associated with high sensitivity to spectral change.

[1] The equivalent situation for such an equation is to have eigenvalues of very different magnitudes.

In a number of papers concerning spectral wave computation, numerical measures are proposed to achieve stable model results economically. WAMDI Group (1988) suggest to use a semi-implicit time integration scheme with a time step that matches the time scale of low-frequency waves. However, numerically stable solution of the resulting system of equations cannot be guaranteed (Press et al., 1993; Hargreaves and Annan (2001)). The ratio of the largest eigenvalue to the smallest eigenvalue of the stiff system of equations, called the condition number, can be so large that even a fully implicit method combined with large time steps precludes a stable solution. For counterexamples, see Hargreaves and Annan (2001). The only remedy is time step reduction or under-relaxation so that the modified system of equations has a spectrum of eigenvalues with a more favourable condition number.

To guarantee numerical stability at relatively large time steps, the so-called action density limiter has been introduced in WAM in the early 1980s (Hersbach and Janssen, 1999). This limiter restricts the rate of change of the energy spectrum at each time step. Because low-frequency waves carry the most energy, it is desirable to solve the balance equation in this part of the spectrum accurately without intervention by the limiter, whereas for high-frequency waves using an equilibrium level is sufficient. Although this approach lacks a rigorous foundation and is not generally applicable or valid, it appears to guarantee numerical stability at relatively large time steps even when these do not match the time scales of wave growth. Moreover, it is believed that the limiter will not affect the stationary solution when convergence is reached. This assumption is widely employed as a justification for the use of limiters. For an overview, we refer to Hersbach and Janssen (1999) and Tolman (2002) and the references quoted therein. Tolman (1992) proposes an alternative to the action density limiter in which the time step is dynamically adjusted where necessary to ensure accurate wave evolution. The calculation of this optimal time step is related to the action density limiter. Further details can be found in Tolman (1992, 2002).

The steady-state solution in the SWAN model is obtained in an iterative manner, which can be

regarded as a time marching method with a pseudo time step. This pseudo time step generally does not match the relatively small time scale in frequency space and consequently, divergence will occur. Therefore, SWAN makes use of the action density limiter to stabilize the iteration process (Booij et al., 1999). However, experience with SWAN has revealed that the limiter acts not only in the equilibrium space, but also in the energy-containing part of the wave spectrum. This finding is also confirmed by Tolman (2002). Furthermore, the limiter appears to be active over almost all spectra in the geographical domain and during the entire iteration process. This activity has been associated with poor convergence behaviour, such as small-amplitude oscillation in frequency space. Ris (1999) demonstrated that stationary SWAN results are influenced by the settings of the action limiter while De Waal (2001) suspects that the limiter acts as a hidden sink in the source term balance under equilibrium conditions. The question to what extent this limiter adversely affects the stationary solution of SWAN has not been addressed previously, and is considered here.

An alternative way to restrict the high rate of change at higher frequencies is under-relaxation, i.e., making smaller updates by means of a much smaller (pseudo) time step (Ferziger and Perić, 1999). Consequently, a limiter may no longer be needed. Although this approach may be suitable to SWAN, it slows down convergence significantly. In this paper, we propose a new method that finds a compromise between fast convergence on the one hand and minimizing the role of the limiter in the energetic part of the spectrum on the other. The key idea to achieve this is to link the extent of updating to the wave frequency—the larger the frequency, the smaller the update. This approach is therefore called frequency-dependent under-relaxation.

The second objective of this paper concerns the formulation and the use of termination criteria required by the iteration procedure in SWAN. In principle, the iterative process should be stopped if the convergence error defined as the difference between the current iterate and the stationary solution is smaller than a prescribed tolerance. At present, the stopping criteria in SWAN make use of the difference between successive iterates as a measure of the error in the converged solution. Experiences in the application of SWAN have shown that the iteration process is often more erratic and typically much slower than reported by Booij et al. (1999). As a result, the current stopping criteria often lead to premature termination of simulations. This is characterised by the fact that, due to the relatively low rate of convergence, the convergence error is larger than the difference between the successive iterates. A stopping criterion is proposed that uses the second derivative or curvature of the series of successive iterates of the calculated wave height. The premise is that this curvature approaches zero upon full convergence.

The outline of this paper is as follows. First, the mathematical framework of SWAN and its numerical implementation are presented in Sections 2 and 3, respectively. Section 4 describes the implementation of two convergence-enhancing measures, namely the action density limiter and the proposed frequency-dependent under-relaxation technique. Section 5 deals with the proposed stopping criterion based on the curvature of the iterate series of the calculated wave height. In Section 6, the impact and effectiveness of the frequency-dependent under-relaxation technique and the new termination criterion are investigated by means of series of SWAN simulations, featuring idealized fetch-limited cases and a depth-limited field case. Section 7 closes with a discussion and conclusions.

2. Model description

In stationary SWAN simulation, the evolution of the action density N is governed by the time-independent wave action balance equation, which reads (Booij et al., 1999):

$$\nabla_{\vec{x}}\left[\left(\vec{c}_g+\vec{U}\right)N\right]+\frac{\partial c_\sigma N}{\partial\sigma}+\frac{\partial c_\theta N}{\partial\theta}=\frac{S_{\mathrm{tot}}}{\sigma}. \quad (1)$$

The first term denotes the propagation of wave energy in two-dimensional geographical $\vec{x}$-space, with $\vec{c}_g$ the group velocity and $\vec{U}$ the ambient current. This term can be recast in Cartesian, spherical or curvilinear coordinates. The second term represents the

effect of shifting of the radian frequency due to variations in depth and mean currents. The third term represents depth-induced and current-induced refraction. The quantities c_σ and c_θ are the propagation velocities in spectral space (σ, θ), with σ and θ indicating the radian frequency and propagation direction, respectively. The right-hand side contains the source term S_{tot} that represents all physical processes that generate, dissipate or redistribute wave energy. In shallow water, six processes contribute to S_{tot}:

$$S_{\text{tot}} = S_{\text{wind}} + S_{\text{nl3}} + S_{\text{nl4}} + S_{\text{wc}} + S_{\text{bot}} + S_{\text{db}}. \tag{2}$$

These terms denote, respectively, energy input by wind, nonlinear transfer of wave energy through three-wave and four-wave interactions and wave decay due to whitecapping, bottom friction and depth-induced wave breaking. Extensive details on the formulations of these processes can be found in Holthuijsen et al. (2004).

To obtain a unique solution of Eq. (1), boundary conditions should be provided. The incoming wave components at the seaward boundaries are specified by a two-dimensional spectrum. The closed boundaries (e.g., a coastline) are fully absorbing for wave energy leaving the geographical domain. The lower and upper boundaries in frequency space are indicated by $\sigma_{\min}$ and $\sigma_{\max}$, respectively. These boundaries are fully absorbing, although a f^{-4} diagnostic tail is added above the high-frequency cut-off, which is used to compute nonlinear wave–wave interactions and for computing integral wave parameters. Since the directional space is a closed circular domain, no boundary conditions are needed.

3. Numerical framework

3.1. Discretization

This section describes the main features of the discretization and solution method of Eq. (1) in SWAN. For more information, we refer to Booij et al. (1999). For the sake of clarity, we restrict ourselves to Cartesian coordinates. Replacing the horizontal gradient operator $\nabla_{\vec{x}}$ by $(\partial/\partial x,\ \partial/\partial y)$ and the geographic velocity vector $\vec{c}_g + \vec{U}$ by (c_x, c_y), Eq. (1) can be rewritten as

$$\frac{\partial c_x N}{\partial x} + \frac{\partial c_y N}{\partial y} + \frac{\partial c_\sigma N}{\partial \sigma} + \frac{\partial c_\theta N}{\partial \theta} = \frac{S_{\text{tot}}}{\sigma}. \tag{3}$$

We choose a rectangular grid with constant mesh sizes Δx and Δy in x- and y-direction, respectively. The spectral space is divided into elementary bins with a constant directional resolution $\Delta\theta$ and a constant relative frequency resolution $\Delta\sigma/\sigma$ (resulting in a logarithmic frequency distribution). We denote the grid counters as $1 \le i \le N_x$, $1 \le j \le N_y$, $1 \le l \le N_\sigma$ and $1 \le m \le N_\theta$ in x-, y-, σ- and θ-spaces, respectively. All variables are located at points (i,j,l,m). We obtain the following approximation of Eq. (3):

$$\begin{aligned}
&\frac{[c_x N]_{i+1/2,j,l,m} - [c_x N]_{i-1/2,j,l,m}}{\Delta x} \\
&\quad + \frac{[c_y N]_{i,j+1/2,l,m} - [c_y N]_{i,j-1/2,l,m}}{\Delta y} \\
&\quad + \frac{[c_\sigma N]_{i,j,l+1/2,m} - [c_\sigma N]_{i,j,l-1/2,m}}{\Delta \sigma} \\
&\quad + \frac{[c_\theta N]_{i,j,l,m+1/2} - [c_\theta N]_{i,j,l,m-1/2}}{\Delta \theta} = \frac{S_{\text{tot}}}{\sigma}\Big|_{i,j,l,m}.
\end{aligned} \tag{4}$$

Note that locations between consecutive counters are indicated by half-indices. Since the unknown values of N and the propagation velocities are only given at points (i,j,l,m), further approximation is needed. In Rogers et al. (2002), a number of higher order upwind schemes are presented for the calculation of the fluxes $c_x N$ at $(i\pm1/2,j,l,m)$ and $c_y N$ at $(i,j\pm1/2,l,m)$. In this paper, however, we employ a first-order upwind scheme in geographical space, since it is sufficiently accurate for nearshore applications[2], relatively cheap and fully monotone, i.e., it cannot to

[2] This is confirmed by some tests with the second order upwind scheme SORDUP (Rogers et al., 2002) and the first order upwind scheme in which no differences are found in the model results obtained with both these schemes.

give rise to spurious oscillations in N in the geographical space:

$$c_x N|_{i+1/2,j,l,m} = \begin{cases} c_x N|_{i,j,l,m}, & c_x|_{i,j,l,m} > 0 \\ c_x N|_{i+1,j,l,m}, & c_x|_{i+1,j,l,m} < 0 \end{cases} \quad (5)$$

and

$$c_y N|_{i,j+1/2,l,m} = \begin{cases} c_y N|_{i,j,l,m}, & c_y|_{i,j,l,m} > 0 \\ c_y N|_{i,j+1,l,m}, & c_y|_{i,j+1,l,m} < 0 \end{cases}. \quad (6)$$

The fluxes at $(i-1/2,j,l,m)$ and $(i,j-1/2,l,m)$ are obtained from Eqs. (5) and (6), respectively, by decreasing the indices by 1 in appropriate manner.

The approximations to the fluxes $c_\sigma N$ at $(i,j,l+1/2,m)$ and $c_\theta N$ at $(i,j,l,m+1/2)$ are usually obtained by combining central differences and a first-order upwind scheme, as follows:

$$c_\sigma N|_{i,j,l+1/2,m} = \begin{cases} \left(1-\frac{1}{2}\mu\right) c_\sigma N|_{i,j,l,m} + \frac{1}{2}\mu c_\sigma N|_{i,j,l+1,m}, & c_\sigma|_{i,j,l,m} > 0 \\ \left(1-\frac{1}{2}\mu\right) c_\sigma N|_{i,j,l+1,m} + \frac{1}{2}\mu c_\sigma N|_{i,j,l,m}, & c_\sigma|_{i,j,l+1,m} < 0 \end{cases} \quad (7)$$

and

$$c_\theta N|_{i,j,l,m+1/2} = \begin{cases} \left(1-\frac{1}{2}\nu\right) c_\theta N|_{i,j,l,m} + \frac{1}{2}\nu c_\theta N|_{i,j,l,m+1}, & c_\theta|_{i,j,l,m} > 0 \\ \left(1-\frac{1}{2}\nu\right) c_\theta N|_{i,j,l,m+1} + \frac{1}{2}\nu c_\theta N|_{i,j,l,m}, & c_\theta|_{i,j,l,m+1} < 0 \end{cases}, \quad (8)$$

where the parameters μ and ν are still to be chosen. Similar expressions can be found for the corresponding fluxes at $(i,j,l-1/2,m)$ and $(i,j,l,m-1/2)$.

For all values $\mu \in [0,1]$ and $\nu \in [0,1]$, a blended form arises between first-order upwind differencing ($\mu=\nu=0$) and central differencing ($\mu=\nu=1$). In the present study, we choose $\mu=\nu=1/2$.

3.2. Solution algorithm

The discretization of the action balance Eq. (1) as described in Section 3.1 yields a system of linear equations that need to be solved. The corresponding matrix structure can take different forms, mainly depending on the propagation of wave energy in the geographic space. For instance, suppose that $c_x>0$ and $c_y>0$, everywhere. Then, the matrix structure has the following form:

$$\begin{bmatrix} \begin{pmatrix} .x.xxx.x.. \\ ..x.xxx.x. \\ ...x.xxx.x \end{pmatrix} & & \\ \begin{pmatrix} ....x..... \\ .....x..... \\ .....x... \end{pmatrix} & \begin{pmatrix} .x.xxx.x.. \\ ..x.xxx.x. \\ ...x.xxx.x \end{pmatrix} & \\ \begin{pmatrix} ....x..... \\ .....x..... \\ .....x... \end{pmatrix} & \begin{pmatrix} ....x..... \\ .....x..... \\ .....x... \end{pmatrix} & \begin{pmatrix} .x.xxx.x.. \\ ..x.xxx.x. \\ ...x.xxx.x \end{pmatrix} \end{bmatrix}. \quad (9)$$

One recognizes that the subblocks on the main diagonal express coupling among the unknowns in the $(\sigma,\ \theta)$-space for each geographic grid point, whereas the off-diagonal subblocks represent coupling across geographical grid points. This system can be solved with a Gauss–Seidel technique in one step (Wesseling, 1992; Press et al., 1993). Generally, the velocities c_x and c_y may have different signs in the geographical domain and hence, more steps are needed. However, it is well known that adapting the ordering of updates of the unknowns N in geographical space to the propagation direction can improve the rate of convergence of the Gauss–Seidel iterative procedure (Wesseling, 1992). This is done as follows. For each iteration, sweeping through grid rows and columns in geographical domain are carried out, starting from each of the four corners of the computational grid. After four sweeps, wave energy has been propagated over the entire geographical domain. During each sweep, only a subset of the unknown values of N are updated depending on the sign of c_x and c_y. For instance, the first sweep starts at the lower left-hand corner and all grid points with $c_x>0$ and $c_y>0$ are updated.

After each propagation update at geographic grid point, an update in the spectral space is made. Since, according to Eqs. (5) and (6), the wave energy at a single spatial location depends on the upwind grid points only, it is sufficient to carry out the update within a 90°-quadrant of the (σ, θ)-space, as illustrated in Fig. 1. Because of the implicit nature of the spectral propagation terms in Eq. (4), a system of equations must be formed. Furthermore, due to the fact that the source term S_{tot} in Eq. (4) is nonlinear in N, linearization is required in order to find a solution. Generally, the term S_{tot} in each bin (l,m) is treated by distinguishing between positive and negative contributions and arranging these in the linear form (Ferziger and Perić, 1999):

$$S_{\text{tot}} = S^{\text{p}}_{\text{tot}} + S^{\text{n}}_{\text{tot}} N, \tag{10}$$

where $S^{\text{p}}_{\text{tot}}$ consists of positive contributions and $S^{\text{n}}_{\text{tot}}$ of negative ones. Both contributions are independent of the solution N at the corresponding bin (l,m). Any negative term that does not contain N as a multiplier is first divided by N obtained from the previous iteration level and then added to $S^{\text{n}}_{\text{tot}}$. This stabilizes the iteration process. Details on the application of this principle to each source term in SWAN can be found in Booij et al. (1999). As such, each difference Eq. (4) using expressions (7), (8) and (10) provides an algebraic relation between N at the corresponding bin and its nearest neighbours:

$$a_{\text{P}} N_{\text{P}} = a_{\text{L}} N_{\text{L}} + a_{\text{R}} N_{\text{R}} + a_{\text{B}} N_{\text{B}} + a_{\text{T}} N_{\text{T}} + b_{\text{P}}, \tag{11}$$

where P corresponds to central bin (l,m) and L(eft), R(ight), B(ottom) and T(op) correspond to ($l-1$,m), ($l+1$,m), (l,$m-1$) and (l,$m+1$), respectively. Furthermore, the coefficients a_k, $k\in\{\text{P, L, R, B, T}\}$ arise from the discretizations of the fluxes $c_\sigma N$ and $c_\theta N$ and b_{P} contains the positive contributions of the source term $S^{\text{p}}_{\text{tot}}$ in Eq. (10) and the updated fluxes $c_x N$ (5) and $c_y N$ (6). Note that coefficient a_P includes $-S^{\text{n}}_{\text{tot}}$.

The linear system of Eq. (11) for all bins within a directional quadrant at a particular geographical point is denoted by

$$\boldsymbol{A}\vec{N} = \vec{b}, \tag{12}$$

where $A\in\mathbb{R}^{K\times K}$ contains the coefficients a_k, $k\in\{\text{P, L, R, B, T}\}$ (and corresponds to a subblock on the main diagonal of Eq. (9)), $\vec{b}\in\mathbb{R}^K$ contains the coefficient b_{P} and boundary values and $\vec{N}\in\mathbb{R}^K$ denotes an algebraic vector containing the unknown action density values. Matrix $\boldsymbol{A}$ is non-symmetric. The dimension K of a directional quadrant equals $N_\sigma\times(1/4)N_\theta$. Note that linearization of the source term (10) enhances diagonal dominance of $\boldsymbol{A}$, thereby improving numerical stability. Also note that neither $\boldsymbol{A}$ nor $\vec{b}$ depends on the unknowns. Each row in the matrix $\boldsymbol{A}$ corresponds to a bin (l,m). The main diagonal contains the coefficients a_{P} and directly to the left and right are the coefficients $-a_{\text{B}}$ and $-a_{\text{T}}$, respectively. The coefficients $-a_{\text{L}}$ and $-a_{\text{R}}$ are on the diagonals that are N_θ positions to the left and right of the main diagonal, respectively.

The solution $\vec{N}$ is given by $\boldsymbol{A}^{-1}\vec{b}$. Since, the only non-zero matrix elements are situated in five diagonals, iterative solution methods that utilize the sparsity of $\boldsymbol{A}$ optimally are very attractive. In SWAN, the solution of Eq. (12) is found by means of an incomplete lower–upper decomposition method followed by an iteration process called the Strongly

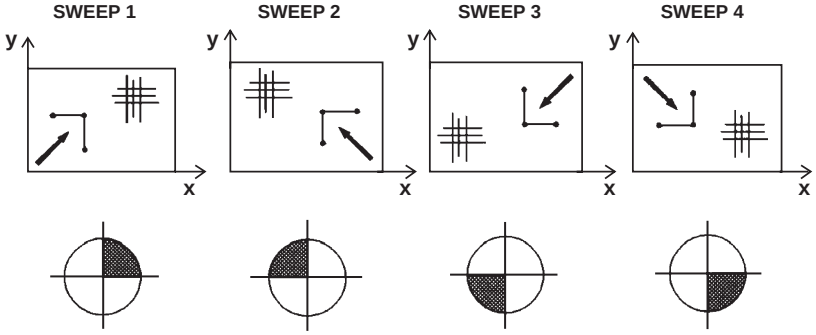

Fig. 1. The solution procedure for wave energy propagation in geographical space with the appropriate directional quadrant (indicated by shaded area) for each of four sweeps.

Implicit Procedure (SIP) (Ferziger and Perić, 1999). This procedure is specifically designed for (non-symmetric) penta-diagonal systems and is relatively fast. Note that in the absence of mean current there are no shifts in the frequency, and consequently the structure of $\boldsymbol{A}$ reduces to a tri-diagonal one, i.e., $a_L=a_R=0$, which can be inverted efficiently with the Thomas algorithm (Press et al., 1993; Ferziger and Perić, 1999).

Due to refraction and nonlinear wave energy transfer, interactions occur between the directional quadrants. To properly take these interactions into account and the fact that we employ the Gauss–Seidel technique and linearization of the source term (10), the quadrant sweeping and the solution of system (12) need to be repeated until some convergence criteria are met. At present, the iteration process runs from $s=1$ to $s=S$ and is terminated if the maximum number of iterations S (usually 15) is reached or the following criteria for the significant wave height H_{m0} and mean relative wave period T_{m01}, as given by

$$H_{m0}=4\sqrt{m_0},\quad T_{m01}=2\pi\frac{m_0}{m_1},\qquad m_j=\int_0^{\infty}\int_0^{2\pi}\sigma^j E(\sigma,\theta)d\sigma d\theta, \tag{13}$$

are both satisfied in at least 98% of all wet grid points (i,j):

$$\frac{|\Delta H^s_{m0}(i,j)|}{H^{s-1}_{m0}(i,j)}<\varepsilon^r_H \text{ or } |\Delta H^s_{m0}(i,j)|<\varepsilon^a_H \tag{14}$$

and

$$\frac{|\Delta T^s_{m01}(i,j)|}{T^{s-1}_{m01}(i,j)}<\varepsilon^r_T \text{ or } |\Delta T^s_{m01}(i,j)|<\varepsilon^a_T. \tag{15}$$

Here, $\Delta Q^s\equiv Q^s-Q^{s-1}$, with Q some quantity. In this study, we use the default values: $\varepsilon^r_H=\varepsilon^r_T=0.02$, $\varepsilon^a_H=0.02$ m and $\varepsilon^a_T=0.2$ s; see Holthuijsen et al. (2004). The rationale behind the use of the integral wave parameters H_{m0} and T_{m01} in the stopping criteria is that these are the output variables typically of interest. The iterative solution procedure is accelerated by calculating a reasonable first guess of the wave field based on second-generation source terms of Holthuijsen and De Boer (1988).

4. Convergence-enhancing measures

As explained in Section 1, many time scales are involved in the evolution of wind waves. The high-frequency waves have much shorter time scales than the low-frequency waves, rendering the system of Eq. (12) stiff. If no special measures are taken, the need to resolve high-frequency waves at very short time scales would result in extreme computational time. For economy, it is desirable that a numerical technique can be used with a large, fixed time step. Moreover, we are mainly interested in the evolution of slowly changing low-frequency waves. For stationary problems, we are interested in obtaining the steady-state solution. Unfortunately, the convergence to the steady state is dominated by the smallest time scale and, in the absence of remedial measures, destabilizing over- and undershoots will prevent solution from converging monotonically during the iteration process. These oscillations arise because of the off-diagonal terms in matrix $\boldsymbol{A}$, which can be dominant over the main diagonal, particularly when the ratio $\sigma_{max}/\sigma_{min}$ is substantially larger than one. As a consequence, convergence is slowed down and divergence often occurs. To accelerate the iteration process without generating instabilities, appropriately small updates must be made to the level of action density.

With the development of the WAM model, a so-called action density limiter was introduced as a remedy to the abovementioned problem. This action limiter restricts the net growth or decay of action density to a maximum change at each geographic grid point and spectral bin per time step. This maximum change corresponds to a fraction of the omni-directional Phillips equilibrium level (Hersbach and Janssen, 1999). In the context of SWAN (Booij et al., 1999), this is

$$\Delta N\equiv\gamma\frac{\alpha_{PM}}{2\sigma k^3 c_g}, \tag{16}$$

where $\gamma\geq 0$ denotes the limitation factor, k is the wave number and $\alpha_{PM}=8.1\times10^{-3}$ is the Phillips constant for a Pierson–Moskowitz spectrum (Komen et al., 1994). Usually, $\gamma=0.1$ (Tolman, 1992)[3]. Denoting the

[3] It is noted here that the effective γ used in SWAN is not equivalent to that of WAM: the former is a factor 2π larger.

total change in $N_{i,j,l,m}$ from one iteration to the next after Eq. (4) by $\Delta N_{i,j,l,m}$, the action density at the new iteration level is given by

$$N^s_{i,j,l,m} = N^{s-1}_{i,j,l,m} + \frac{\Delta N_{i,j,l,m}}{|\Delta N_{i,j,l,m}|} \min\{|\Delta N_{i,j,l,m}|, \Delta N\}. \tag{17}$$

For wave components at relatively low frequencies, Eq. (17) yields the pre-limitation outcome of Eq. (4), because, for these components, the pseudo time step matches the time scale of their evolution. For high-frequency waves, however, Eq. (17) gives the upper limit for the spectrum to change per iteration due to the limiter (16). For typical coastal engineering applications, it is sufficient to compute the energy-containing part of the wave spectrum accurately. In other words, action densities near and below the spectral peak should not be imposed by the limiter (16). However, our experiences with SWAN have shown that the limiter is active even close to the peak. Furthermore, during the entire iteration process, the limiter is typically active at almost every geographic grid point, as will be shown in Section 6.

The alternative measure to enhance the convergence of the stable iteration process considered here is so-called false time stepping (Ferziger and Perić, 1999). Under-relaxation terms representing the rate of change are introduced to enhance the main diagonal of $\boldsymbol{A}$ and thus stabilize the iteration process. The system of Eq. (12) is replaced by the following, iteration-dependent system

$$\frac{\vec{N}^s - \vec{N}^{s-1}}{\tau} + A\vec{N}^s = \vec{b} \tag{18}$$

with τ a pseudo time step. The first term of Eq. (18) controls the rate of convergence of the iteration process in the sense that smaller updates are made due to decreasing τ, usually at the cost of increased computational time. To deal with decreasing time scales at increasing wave frequency, the amount of under-relaxation is enlarged in proportion to frequency. This allows a decrease in the computational cost of under-relaxation, because at lower frequencies larger updates are made. This frequency-dependent under-relaxation can be achieved by setting $\tau^{-1}=\alpha\sigma$, where α is a dimensionless parameter. The parameter α will play an important role in determining the convergence rate and stability of the iteration process. Substitution in Eq. (18) gives

$$(\boldsymbol{A} + \alpha\sigma\boldsymbol{I})\vec{N}^s = \vec{b} + \alpha\sigma\vec{N}^{s-1}. \tag{19}$$

When the steady state is reached (i.e., $s\rightarrow\infty$), system (19) solves $\boldsymbol{A}\vec{N}^{\infty} = \vec{b}$ since, $\vec{N}^{\infty}$ is a fixed point of Eq. (19).

Suitable values for α must be determined empirically and thus robustness is impaired. For increasing values of α, the change in action density per iteration will decrease in the whole spectrum. The consequence of this is twofold. Firstly, it allows a much broader frequency range in which the action balance Eq. (4) is actually solved without distorting convergence properties. Secondly, the use of the limiter will be reduced because more density changes will not exceed the maximum change (16). Clearly, this effect may be augmented by increasing the value of γ in Eq. (16).

To allow proper calculation of the second-generation first guess of the wave field (see Section 3.2), under-relaxation is temporarily disabled (α=0) during the first iteration. Whereas this measure is important in achieving fast convergence, it does not affect stability, since the second-generation formulations do not require stabilization.

5. Stopping criteria

In general, the iterative method should be stopped if the approximate solution is accurate enough. A good termination criterion is very important, because if the criterion is too weak the solution obtained may be useless, whereas if the criterion is too severe the iteration process may never stop or may cost too much work. Experiences with SWAN have shown that the present criteria (14) and (15) are often not strict enough to obtain accurate results after termination of the iterative procedure. Thus, criteria (14) and (15) are necessary but not sufficient. It was found that the iteration process can converge so slowly that at a certain iteration s the difference between the successive iterates, $H^s_{m0}-H^{s-1}_{m0}$, can be small enough to meet the convergence criteria, causing the iteration process to stop, even though the converged solution has not yet been found. In particular, this happens when

convergence is non-monotonic such that the process is terminated at local maxima or minima that may not coincide with the converged solution.

Furthermore, it became apparent that, unlike H_{m0}, the quantity T_{m01} is not an effective measure of convergence. It was found that the relative error in T_{m01}, i.e. $|T^s_{m01}-T^{s-1}_{m01}|/T^{s-1}_{m01}$, does not monotonically decrease near convergence, but keeps oscillating during the iteration process. This behaviour is due to small variations in the spectrum at high frequencies, to which T_{m01} is sensitive. This behaviour is problematic when any form of stricter stopping criterion is developed based on T_{m01}. Therefore, in the improved termination criterion proposed in this paper, T_{m01} has been abandoned as a convergence measure and only H_{m0}, which displays more monotonic behaviour near convergence, is retained.

Stiffness and nonlinearity of the action balance equation are found to yield less rapid and less monotone convergence. Ferziger and Perić (1999) explain the slow convergence in terms of the eigenvalue or spectral radius of the iteration process generating the sequence $\{\phi^0, \phi^1, \phi^2,\ldots\}$. They show that the actual solution error is given by

$$\phi^\infty - \phi^s \approx \frac{\phi^{s+1}-\phi^s}{1-\rho}, \tag{20}$$

where ϕ^∞ denotes the steady-state solution and ρ is the spectral radius indicating the rate of convergence. The smaller the ρ, the faster the convergence. This result shows that the solution error is larger than the difference between successive iterates. Furthermore, the closer ρ is to 1, the larger the ratio of solution error to the difference between successive iterates. In other words, the lower the rate of convergence of the iteration process, the smaller this difference from one iteration to the next must be to guarantee convergence. The stopping criterion of SWAN could be improved by making the maximum allowable relative increment in H_{m0} a function of its spectral radius instead of imposing a fixed allowable increment. By decreasing the allowable relative increment as convergence is neared, it would be possible to delay run termination until a more advanced stage of convergence. Such a stopping criterion was used by, e.g., Zijlema and Wesseling (1998). This criterion is adequate if the iteration process converges in a well-behaved manner and $\rho<1$ for all iterations. However, due to nonlinearities SWAN typically does not display such smooth behaviour. Therefore, this criterion may be less suited for SWAN.

An alternative way to evaluate the level of convergence is to consider the second derivative or curvature of the curve traced by the series of iterates (iteration curve). Since the curvature of the iteration curve must tend towards zero as convergence is reached, terminating the iteration process when a certain minimum curvature has been reached would be a robust break-off procedure. The curvature of the iteration curve of H_{m0} may be expressed in the discrete sense as

$$\Delta\left(\Delta\tilde{H}^s_{m0}\right)^s = \tilde{H}^s_{m0} - 2\tilde{H}^{s-1}_{m0} + \tilde{H}^{s-2}_{m0}, \tag{21}$$

where $\tilde{H}^s_{m0}$ is some measure of the significant wave height at iteration level s. To eliminate the effect of small amplitude oscillations on the curvature measure, we define $\tilde{H}^s_{m0} \equiv \left(H^s_{m0} + H^{s-1}_{m0}\right)/2$. The resulting curvature-based termination criterion at grid point (i,j) is then

$$\frac{\left|H^s_{m0}(i,j) - \left(H^{s-1}_{m0}(i,j) + H^{s-2}_{m0}(i,j)\right) + H^{s-3}_{m0}(i,j)\right|}{2H^s_{m0}(i,j)} < \varepsilon_C,$$
$$s = 3,4,.., \tag{22}$$

where ε_C is a given maximum allowable curvature. The curvature measure is made non-dimensional through normalization with H^s_{m0}. Condition (22) must be satisfied in at least 98% of all wet grid points before the iterative process stops. This curvature requirement is considered to be the primary criterion.

However, the curvature passes through zero between local maxima and minima and, at convergence, the solution may oscillate between two constant levels due to the action limiter, whereas the average curvature is zero. As safeguard against such a situation, the weaker criterion (14) is retained in addition to the stricter criterion (22).

6. Simulations

In this section, the numerical implementations described in Sections 4 and 5 are investigated by means of numerical simulations. To explore the comparative performance of the convergence-enhanc-

ing methods, two situations are considered: idealized, fetch-limited wave growth and the field case of Lake George, Australia (Young and Verhagen, 1996), which represents depth-limited wave growth. In these tests the convergence behaviour is of interest. Following this consideration of iteration behaviour, the attention is turned to the application of stopping criteria. The performance of the present and newly proposed criteria are compared for the field experiment of Lake George.

6.1. Convergence behaviour studies

The first situation investigated is that of deep-water, fetch-limited, idealized wave growth over a fetch of 25 km, for spatially uniform wind with speeds of U_{10}=10 and 30 m/s. The depth is set to 10^5 m. Simulations were conducted in one-dimensional, stationary mode, using a spatial discretization of Δx=100 m. The frequencies ranged from $f_{\min}$=0.04 Hz to $f_{\max}$=1.0 Hz and are discretized into 34 bins on a logarithmic scale ($\Delta f/f \approx 0.1$). The wave directions are discretized into 36 sectors each of 10 degrees. For simulations at U_{10}=10 m/s the frequency range was shifted to 0.06–3.0 Hz, with a discretization of Δf=0.12f, to accommodate high-frequency growth. The simulations were conducted using the default third-generation physics formulations of SWAN (see Holthuijsen et al., 2004). For the iteration behaviour up to convergence and beyond, the stopping criteria (14) and (15) were disabled and iteration was continued up to a sufficiently large chosen maximum. The method of model convergence enhancement was varied for various runs. The following approaches were considered: (a) the application of the present default action limiter in SWAN (α=0.0, γ=0.1), (b) using frequency-dependent under-relaxation in addition to the action limiter (α, γ>0) and (c) applying frequency-dependent under-relaxation without the action limiter (α>0, $\gamma=\infty$). Various values of the under-relaxation parameter α were considered. To serve as a benchmark in these comparisons, the test case of idealized wave growth was also calculated in nonstationary mode, using a very small time step of Δt=1 s and no limiter[4]. The corresponding results, depicted in Fig. 2, can be regarded as the true numerical solution of the problem. Note that the stationary solution is reached after approximately 7000 and 4000 time steps for the U_{10}=10 and 30 m/s cases, respectively.

Firstly, the convergence behaviour of SWAN is discussed when using the default value of the action limiter (γ=0.1) and various moderate levels of under-relaxation (α=0.00–0.05. In these simulations, the run with α=0 represents the default SWAN result (base case). Fig. 3 presents the iteration behaviour of H_{m0} for U_{10}=10 and 30 m/s at a fetch of 12.5 km. As reference, the equilibrium-level results of the nonstationary benchmark simulations have been added. Fig. 4 shows the lowest frequency bin at which the limiter was active during the simulation, for the various settings of α. It should be noted that this minimum appears to be more or less independent of the spectral direction component. With α=0 convergence is fast (see Fig. 3) but the limiter was heavily used to obtain this fast convergence (Fig. 4). Note also the persistent small oscillations in the curves with α=0. Furthermore, the limiter was active throughout both the U_{10}=10 and 30 m/s simulations, up to period bins above the highest values of T_{m01} respectively reached. In comparison, the curves for α>0 in Fig. 3 show three effects of under-relaxation. First, under-relaxation considerably slows down the speed of convergence, with the number of iterations required for convergence increasing with increasing values of α. Second, the iterative behaviour is smoothed by under-relaxation. Third, the overshoot in significant wave height during iteration is reduced. Another advantage of under-relaxation is seen in the altered activity of the limiter, as shown in Fig. 4. At increasing levels of under-relaxation, the lowest frequency at which the updates are limited increases. This implies that the influence of the limiter on model results is reduced. In terms of numerical accuracy, the solution of the simulations with α>0 are in agreement with those of the nonstationary benchmark simulations (especially for higher values of α), whereas the α=0 simulation slightly over-estimates H_{m0}.

Considering the decreasing time scales at higher frequencies, convergence should be achievable solely by slowing down the updates of spectral energy change. This can be achieved by applying strong frequency-dependent under-relaxation. During such

[4] For U_{10}=10 m/s, the limiter (16) with γ=1.0 was necessary to maintain stability at the highest frequency bin (3.0 Hz), but its impact was limited to this bin.

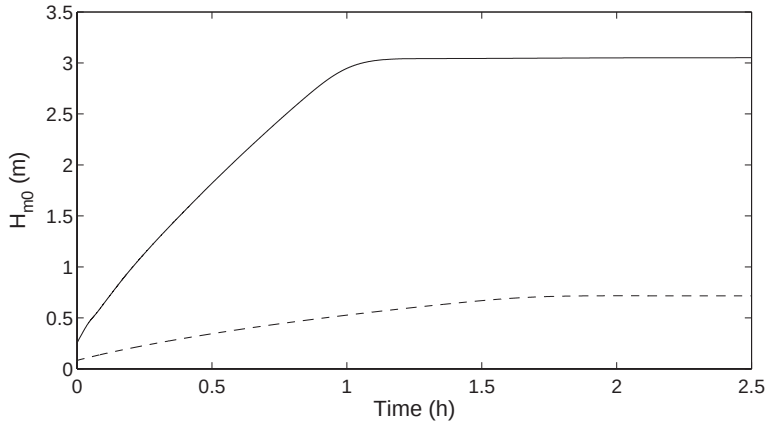

Fig. 2. Deep-water, fetch-limited wave growth for wind speeds of U_{10}=10 (dashed line) and 30 m/s (solid), at fetch=12.5 km. Results for nonstationary SWAN with Δt=1 s and no limiter.

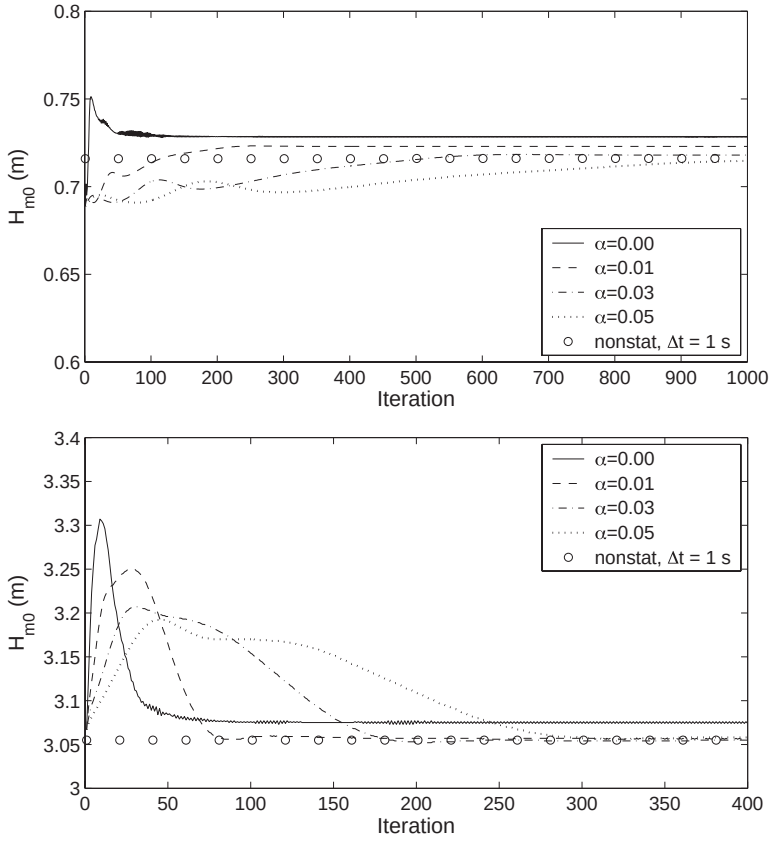

Fig. 3. Convergence behaviour of H_{m0} in deep-water, fetch-limited simulations for wind speeds U_{10}=10 (top panel) and 30 m/s (bottom panel), at fetch=12.5 km. Results for SWAN with γ=0.1 and α=0.0–0.05. Also shown is nonstationary SWAN with Δt=1 s.

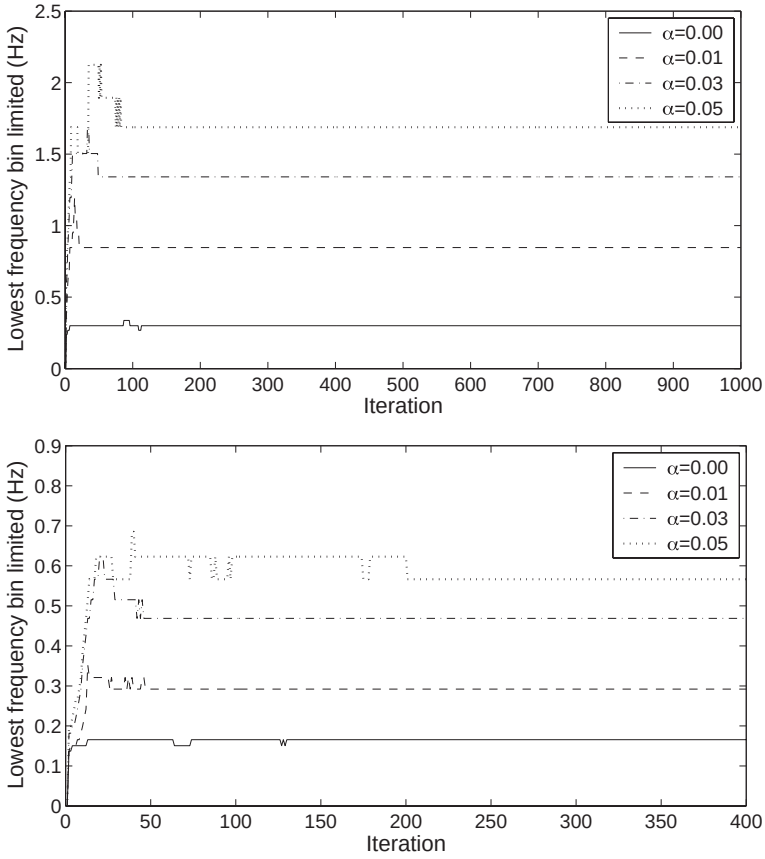

Fig. 4. Lowest frequency bin at which limiter is active, as a function of iteration level. Results for deep-water, fetch-limited simulations for wind speeds U_{10}=10 (top panel) and 30 m/s (bottom panel), with γ=0.1 and α=0.0–0.05.

simulations, stable behaviour should be possible even with the limiter deactivated. Therefore, a next set of simulations was done for the idealized, fetch-limited case, with under-relaxation of up to α=0.20, with the limiter deactivated. Figs. 5 and 6 present simulation results for U_{10}=10 m/s and 30 m/s in which the nonstationary benchmark results are again displayed. The curves with α=0 again represent the standard SWAN result, obtained with the limiter (γ=0.1). The remaining curves (α=0.10 and 0.20) show the effect of strong under-relaxation, without the use of the limiter ($\gamma=\infty$). At a relatively low level of under-relaxation (α=0.10), stability could not be achieved without the limiter. This represents the situation in which the pseudo time step still exceeds the time scales of spectral change. However, for intensified under-relaxation (α=0.20) the simulation does indeed remain stable, even in the absence of the limiter. As seen before, under-relaxation results in longer convergence times. For the strong under-relaxation applied here, convergence was only reached after 1000 and 4000 iterations for U_{10}=30 m/s and 10 m/s, respectively. It should be noted that fewer iterations are needed for the higher wind speed. This is due to the fact that the ratio $\sigma_{max}/\sigma_{min}$ is half that at U_{10}=10 m/s case, so that the corresponding system of equations is less stiff, thus improving the convergence rate (see Section 4). Considering the growth curves (Fig. 6), excellent agreement is found between the results of the strongly under-relaxed, unlimited simulations and those of the nonstationary benchmark simulations. This would suggest that by using frequency-dependent under-relaxation, a very good approximation of the true numerical solution is obtained.

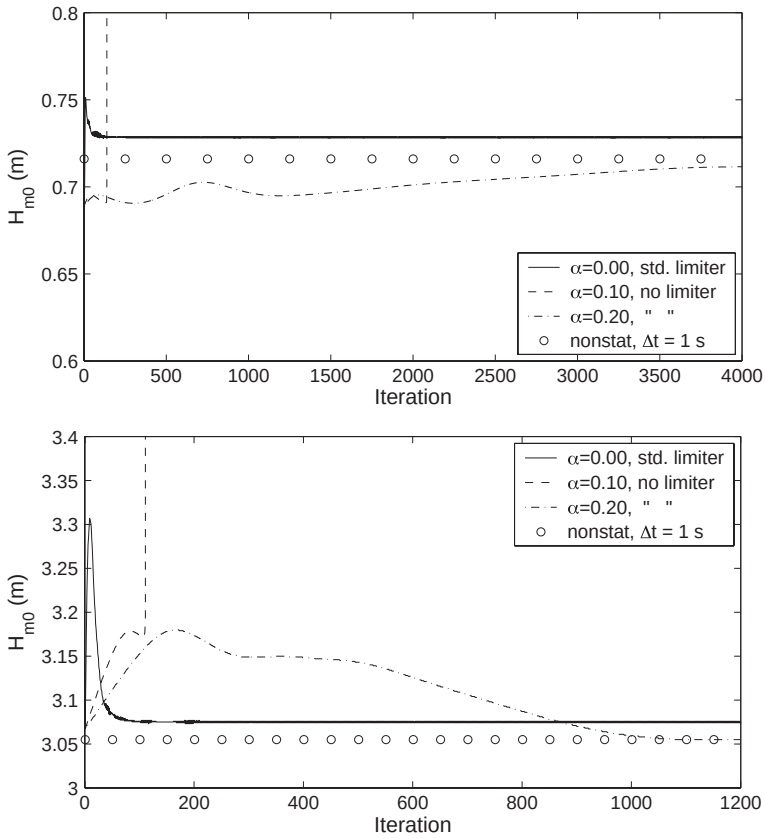

Fig. 5. Convergence behaviour of H_{m0} in deep-water, fetch-limited simulations for wind speeds U_{10}=10 (top panel) and 30 m/s (bottom panel), at fetch=12.5 km. Results for SWAN without limiter ($\gamma=\infty$) and various large under-relaxation factors (α=0.10–0.20). Also shown are stationary SWAN with γ=0.1 and α=0, and nonstationary SWAN with Δt=1 s.

The results of the unrelaxed, limited simulations also agree well with those of the other two methods, with only a slight over-estimation of H_{m0} visible. This is due to the fact that the limiter is always applied at frequencies where low-frequency energy resides (see Fig. 4). This implies that the limiter will systematically impact the solution. Since the limiter restricts both positive and negative changes to the spectrum, it can be both a source or sink of wave energy. It was observed that in the first few iterations the limiter (γ=0.1) allows slightly larger growth of high-frequency energy compared to the frequency-dependent under-relaxation and nonstationary approaches. This energy is partly dissipated by whitecapping on a relatively long time scale and partly transported to lower frequencies by four-wave interactions on a significantly shorter time scale. At the point of convergence, it was found that the resulting spectra agree very well, except for a small amount of energy on the low-frequency face of the peak, accumulated in the spectrum of the simulation using the action limiter. It is this accumulated energy which accounts for the observed small over-estimation of H_{m0} results.

Considering the results of the two sets of simulations described above, the setting α=0.05, γ=0.5 was chosen as a practical combination of frequency-dependent under-relaxation and the action limiter. With this combination, which lies between the extremes applied in the first and second simulation sets, the advantages of improved numerical accuracy and smooth convergence are obtained, while retaining a relatively fast convergence speed compared to the extreme example (α=0.2, $\gamma=\infty$). The results of fetch-

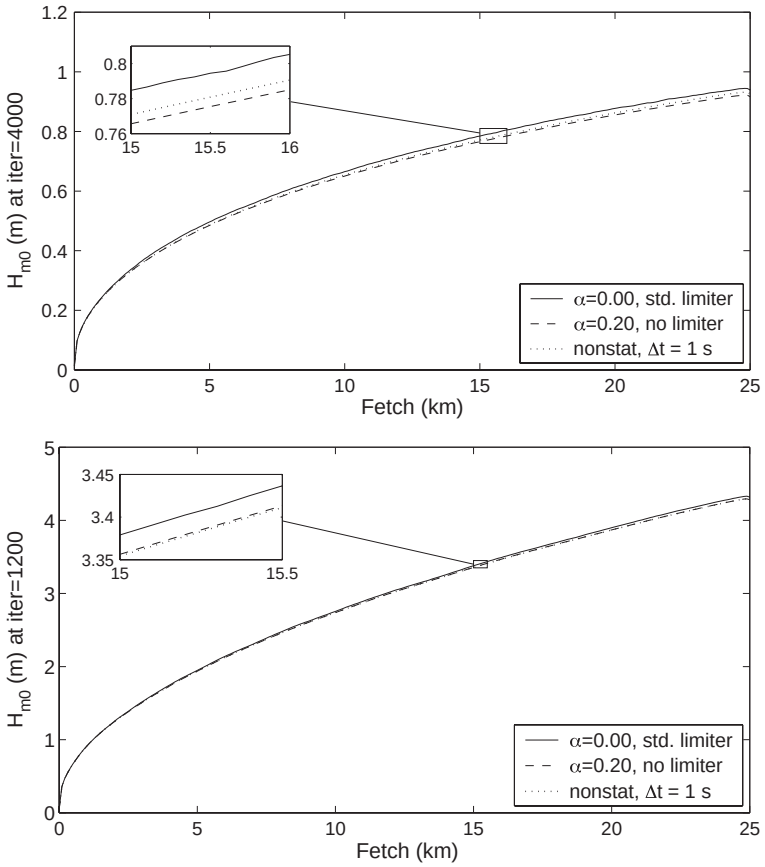

Fig. 6. Growth curves of H_{m0} in deep-water, fetch-limited simulations for wind speeds of U_{10}=10 (top panel) and 30 m/s (bottom panel). Results for stationary SWAN with limiter, for α=0.20 without limiter and nonstationary SWAN with Δt=1 s.

limited simulation with this setting are essentially similar to the results of the setting α=0.05, γ=0.1. Next, the performance of this setting is investigated for practical application in the field case of Lake George.

The Lake George field experiment of Young and Verhagen (1996) represents near-idealized, depth-limited wave growth. Lake George is a shallow lake (depth about 2 m) with a nearly flat bottom and is approximately 20 km long and 10 km wide. Wave spectra were measured along the North–South axis of the lake using an array of eight gauges. The simulation of one representative case is presented here, namely case 'f41lak02' of the ONR Test Bed (Ris et al., 2002). In this case, wave growth is caused by a northerly wind of U_{10}=10.8 m/s. The simulations were conducted in two-dimensional stationary mode using a spatial discretization of $\Delta x=\Delta y \approx 200$ m, a directional discretization of 10°, a frequency range of 0.125 to 1.0 Hz and a frequency discretization of Δf=0.1f. The simulations were conducted using the default third-generation physics formulations of SWAN. Iteration was continued up to convergence and beyond, with the stopping criteria (14) and (15) disabled. Simulations were conducted with two settings of the convergence-enhancing methods, namely the default action density limiter (α=0.0, γ=0.1) and the combination of under-relaxation and limiter α=0.05 and γ=0.5.

Figs. 7 and 8 present comparative simulation results of the two convergence-enhancing methods after 500 iterations. It is striking that both in terms of spectra (Fig. 7) and integral parameters (Fig. 8) there is virtually no difference between the results pro-

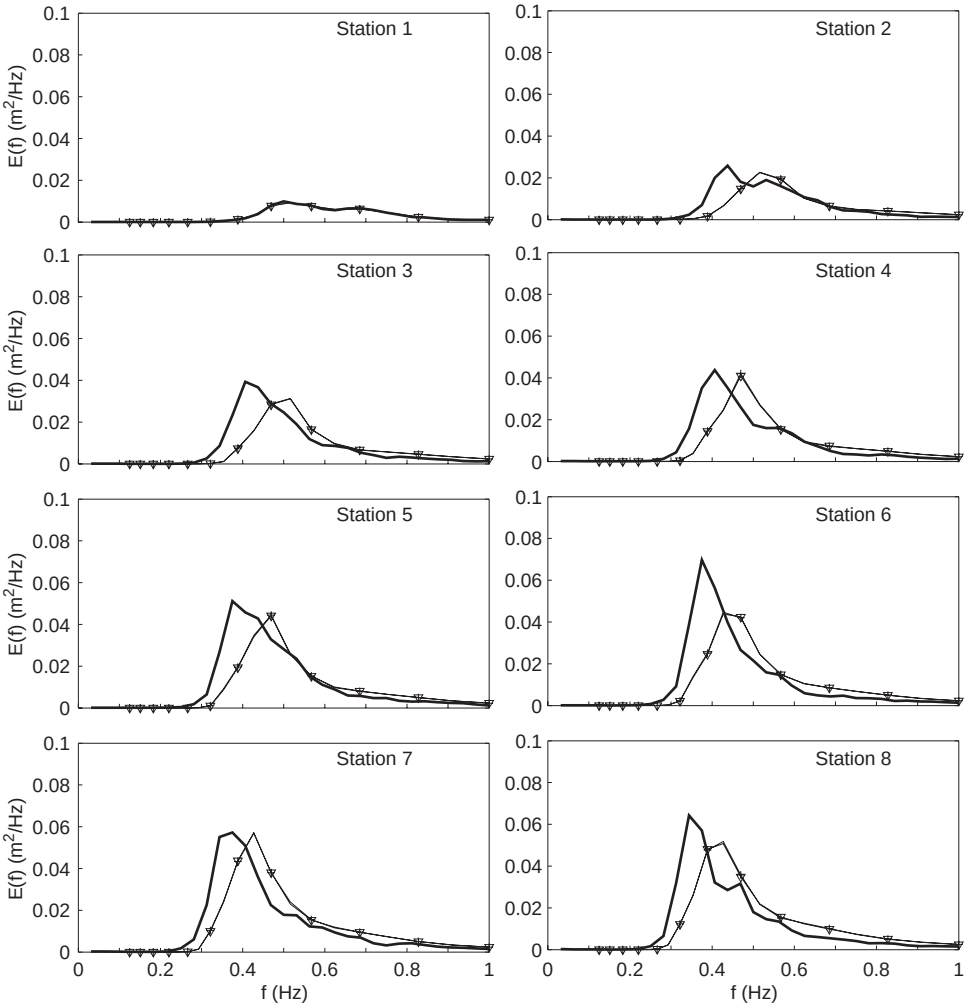

Fig. 7. Lake George field experiment of near-idealized, depth-limited wave growth. 1D spectra obtained with α=0.0 and γ=0.1 after 500 iterations (plusses), with α=0.05 and γ=0.5 after 500 iterations (triangles) and observations of Young and Verhagen (1996) (thick line). Note: all plusses virtually coincide with the triangles and for that reason are not separately visible.

duced without under-relaxation (α=0) and the action limiter at γ=0.1 and with under-relaxation (α=0.05) and the action limiter at γ=0.5. This correspondence would indicate that also here the action limiter has minimal influence on the simulation results. When comparing the two sets of simulation results to the observations, it is seen that total energy levels compare very well, but that there is a consistent underprediction of peak period. The latter is a well-known shortcoming of SWAN, which is still actively being researched (Ris et al., 1999; Rogers et al., 2003).

6.2. Termination of a simulation

In Section 6.1 it was shown that in simulations of the Lake George field case the default action limiter and frequency-dependent under-relaxation convergence-enhancing methods yielded very similar results. By making use of under-relaxation in this way, it has been established that the default action limiter has little influence on model outcome. In these simulations, however, the focus was on the final, converged solution, and 500 iterations were allowed to achieve this. The question that remains is whether, in practical

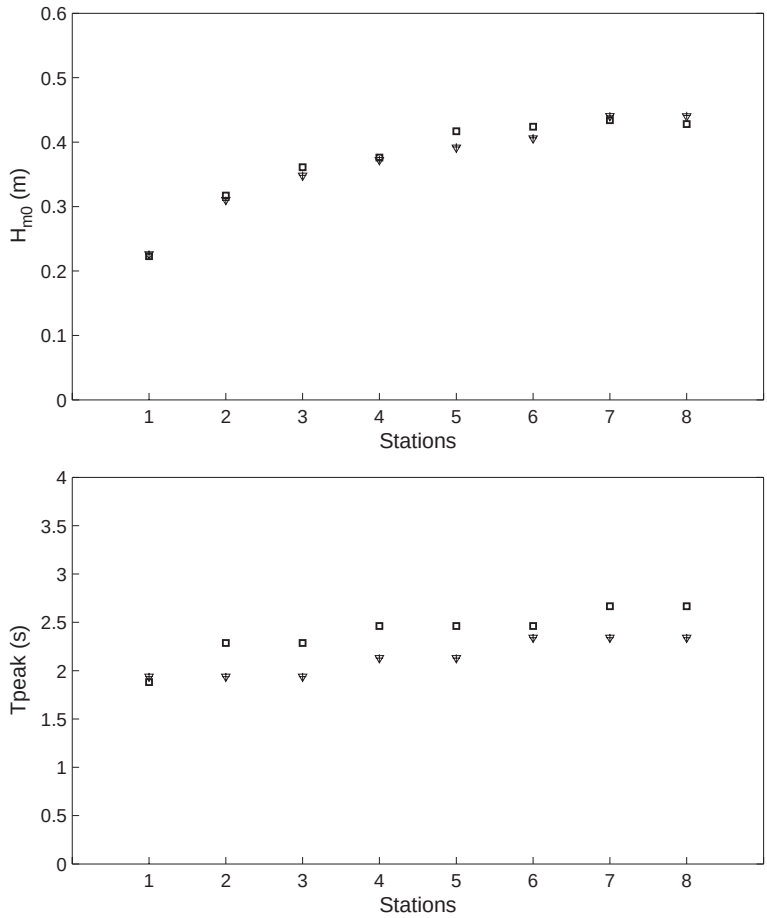

Fig. 8. Lake George field experiment of near-idealized, depth-limited wave growth. Wave height and peak period obtained with α=0.0 and γ=0.1 after 500 iterations (plusses), with α=0.05 and γ=0.5 after 500 iterations (triangles) and observations of Young and Verhagen (1996) (squares). Note: all plusses virtually coincide with the triangles and for that reason are not separately visible.

applications in which a stopping criterion and significantly fewer iterations are used, such well-converged results are obtained.

This section compares the current default stopping criteria of SWAN with the newly proposed criteria in Section 5. The simulation of the Lake George case 'f41lak02' was repeated using the same settings as before, but this time using only the default action limiter (α=0.0, γ=0.1). Using this model set-up, a first set of simulations was conducted with the default stopping criteria (14) and (15). A second set of simulations was conducted with the newly proposed curvature-based criteria (14) and (22), using ε_H^r=0.02, ε_H^a=0.02 m and ε_C=0.0001. In a wide range of field cases of the ONR Test Bed, these tolerance values appears to ensure good accuracy, with the criterion (22) being dominant.

Fig. 9 presents the iteration behaviour of the Lake George simulation with the default action limiter (α=0.0, γ=0.1) at Station 8, the furthest observation point downwind. Superimposed on Fig. 9 are the termination points determined by the default stopping criteria (14) and (15) and the proposed criteria (14) and (22). The default stopping criteria, currently used in SWAN, prematurely terminates the simulation at iteration No. 6, resulting in about 10% underprediction of the converged value of H_{m0}. In contrast to this, the curvature-based criteria terminate the simulation at iteration No. 30, at which point the solution of H_{m0} has converged. Fig. 10 shows the normalized curva-

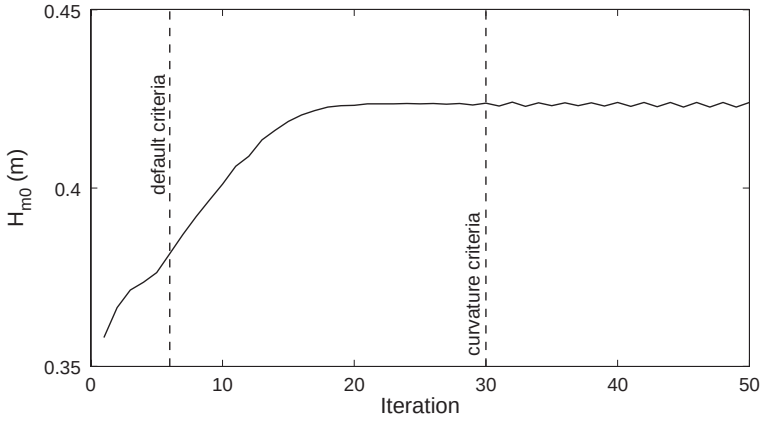

Fig. 9. Lake George field experiment of near-idealized, depth-limited wave growth (Station 8). Iteration behaviour of SWAN with α=0.0 and γ=0.1 with positions of run termination using default stopping criteria (14) and (15) with ε_H^r=ε_T^r=0.02, ε_H^a=0.02 m and ε_T^a=0.2 s (6 iterations) and criteria (14) and (22) with ε_H^r=0.02, ε_H^a=0.02 m and ε_C=0.0001 (30 iterations).

ture measure (22) calculated at Station 8 as a function of iteration level, as well as the limiting normalized curvature value, ε_C=0.0001. It can be seen that the curvature measure consistently reduces throughout the iteration process. After the 24th iteration the curvature measure remains below the given ε_C, meeting the convergence test at this location; at iteration No. 30 this was the case at 98% of all wet grid points, which terminated the iteration process.

Figs. 11 and 12 present the resulting spectra and integral parameters at the eight observation points. These figures confirm the improvement achieved by using the proposed stopping criteria (14) and (22). The results achieved with these criteria are similar to those obtained in the fully converged results of Section 6.1.

7. Discussion and conclusions

In this study, two numerical aspects of the stationary third-generation wind wave model SWAN have been considered, namely convergence-enhancing measures and stopping criteria. Their application has been shown for idealized and nearly idealized fetch- and depth-limited wave growth situations, in which

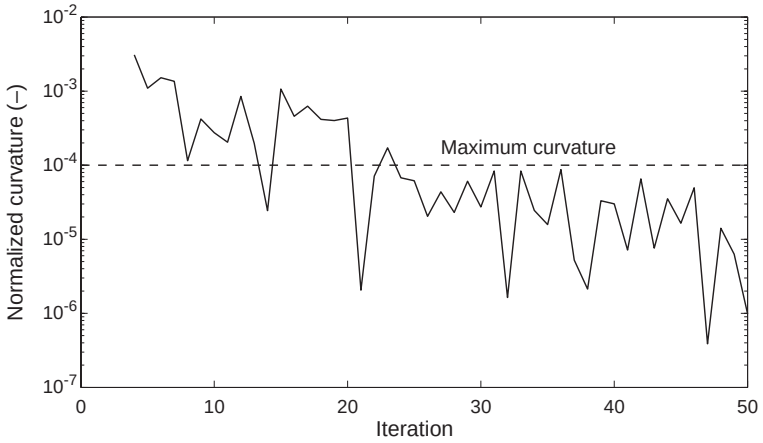

Fig. 10. Lake George field experiment of near-idealized, depth-limited wave growth (Station 8). Curvature measure (22) vs. iteration number, with given maximum allowable curvature ε_C.

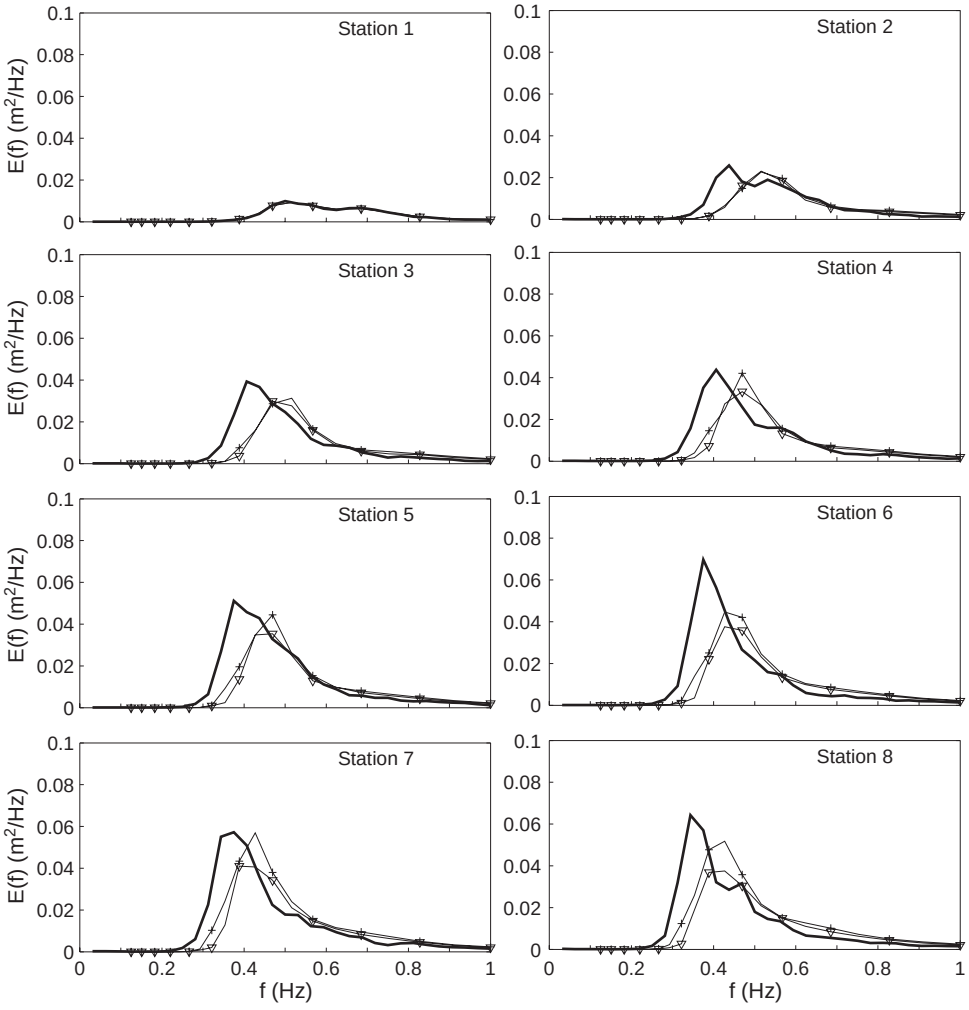

Fig. 11. Lake George field experiment of near-idealized, depth-limited wave growth. 1D spectra obtained with α=0.0, γ=0.1 and default stopping criteria (14) and (15) with $\varepsilon_H^r=\varepsilon_T^r$=0.02, ε_H^a=0.02 m and ε_T^a=0.2 s (6 iterations, triangles), with α=0.0, γ=0.1 and criteria (14) and (22) with ε_H^r=0.02, ε_H^a=0.02 m and ε_C=0.0001 (30 iterations, plusses) and observations of Young and Verhagen (1996) (thick line).

the source terms of wind input, whitecapping and nonlinear four-wave interaction are dominant.

This study has shown that a stable solution is possible without use of the action limiter, using the frequency-dependent under-relaxation technique. It was shown that this method achieves smoother iteration behaviour than the action limiter, although it is more computationally expensive. Because of this increased computational cost, the method of frequency-dependent under-relaxation is probably not well suited to practical application (e.g., forecasting). On the other hand, it can be considered as an important numerical aid for scientific applications.

Since frequency-dependent under-relaxation imposes no external limitation on wave growth, it can be considered a true numerical solution to the formulations of physics in SWAN. This has been confirmed by the fact that the results of this method are in excellent agreement with those of nonstationary calculations using a very small time step (Δt=1 s) and no limiter. As such, it is a significant discovery that the results produced by the action limiter differ very little from those of frequency-dependent under-

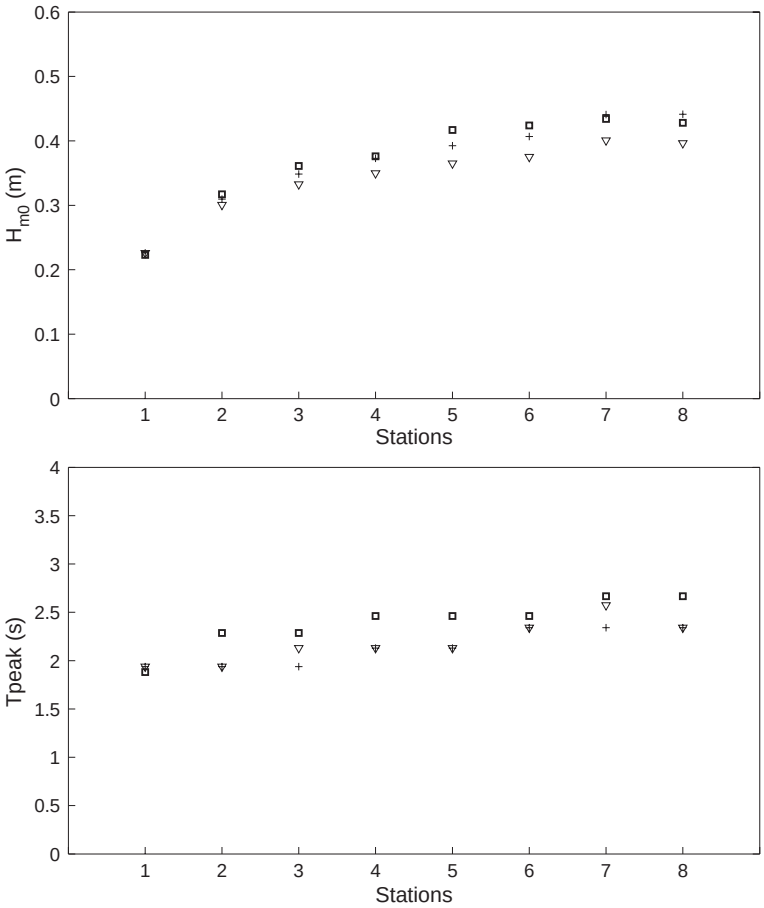

Fig. 12. Lake George field experiment of near-idealized, depth-limited wave growth. Wave height and peak period obtained with α=0.0, γ=0.1 and default stopping criteria (14) and (15) with $\varepsilon_H^r=\varepsilon_T^r$=0.02, ε_H^a=0.02 m and ε_T^a=0.2 s (6 iterations, triangles), with α=0.0, γ=0.1 and termination criteria (14) and (22) with ε_H^r=0.02, ε_H^a=0.02 m and ε_C=0.0001 (30 iterations, plusses) and observations of Young and Verhagen (1996) (squares).

relaxation, for a wide range of stationary cases (including others not presented here). This would suggest that the limiter may not have a significant impact on stationary model solutions.

The finding that, when properly converged, the results of frequency-dependent under-relaxation simulations do not differ noticeably from the results of action limiter simulations implies that, at present, there is little gain in applying under-relaxation to practical applications. However, it was shown that current SWAN simulations tend to be prematurely terminated by the default stopping criteria, so that the true converged solution is not reached. This has called for the development of the newly proposed stricter stopping criterion based on the curvature of the series of successive iterates of the significant wave height. It has been shown that this termination criterion is significantly better at locating the point of convergence than the current default criteria.

This study has provided improved understanding of the impact of the numerics in SWAN on its performance. This makes it possible to make a clearer distinction between inaccuracies due to numerics and those due to approximations in the formulations of physical processes. An example of this is the remaining underprediction of peak wave period in the model results of Lake George (Figs. 7 and 8). With the improved understanding of numerical influence,

these discrepancies can, with greater certainty, be ascribed to shortcomings in the formulations of model physics.

Acknowledgements

Parts of this study are supported by the National Institute for Coastal and Marine Management/RIKZ of the Ministry of Transport, Public Works and Water Management through the project RKZ-1124.

References

Booij, N., Ris, R.C., Holthuijsen, L.H., 1999. A third-generation wave model for coastal regions: 1. Model description and validation. J. Geophys. Res. 104 (C4), 7649–7666.

De Waal, J.P., 2001. Wave growth limit in shallow water. Proc. 4th Int. Symp. Waves, pp. 560–569.

Ferziger, J.H., Perić, M., 1999. Computational methods for fluid dynamics, 2nd edition. Springer-Verlag, Berlin.

Hargreaves, J.C., Annan, J.D., 2001. Comments on "Improvement of the short-fetch behavior in the wave ocean model (WAM)". J. Atmos. Ocean. Technol. 18, 711–715.

Hersbach, H., Janssen, P.A.E.M., 1999. Improvement of the short-fetch behavior in the wave ocean model (WAM). J. Atmos. Ocean. Technol. 16, 884–892.

Holthuijsen, L.H., De Boer, S., 1988. Wave forecasting for moving and stationary targets. In: Schrefler, B.Y., Zienkiewicz, O.C. (Eds.), Computer Modelling in Ocean Engineering. A.A. Balkema, Rotterdam, The Netherlands, pp. 231–234.

Holthuijsen, L.H., Booij, N., Ris, R.C., Haagsma, I.J.G., Kieftenburg, A.T.M.M., Kriezi, E.E., Zijlema, M., Van der Westhuysen, A.J., 2004. SWAN—User manual. Delft University of Technology, Environmental Fluid Mechanics Section, available from http://www.fluidmechanics.tudelft.nl/swan/index.htm (Version 40.31, February 2004).

Komen, G.J., Cavaleri, L., Donelan, M., Hasselmann, K., Hasselmann, S., Janssen, P.A.E.M., 1994. Dynamics and Modelling of Ocean Waves. Cambridge University Press, New York.

Press, W.H., Flannery, B.P., Teukolsky, S.A., Vetterling, W.T., 1993. Numerical recipes in Fortran 77. The art of scientific computing, 2nd edition. Cambridge University Press, New York (available from http://www.nr.com).

Ris, R.C., 1999. Model convergence of SWAN in the Westerschelde estuary WL|Delft Hydraulics, Report H3496.

Ris, R.C., Holthuijsen, L.H., Booij, N., 1999. A third-generation wave model for coastal regions: 2. Verification. J. Geophys. Res. 104 (C4), 7667–7681.

Ris, R.C., Holthuijsen, L.H., Smith, J.M., Booij, N., Van Dongeren, A.R., 2002. The ONR Test Bed for coastal and oceanic wave models. Proc. 28th Int. Conf. Coastal Engng., ASCE, pp. 380–391.

Rogers, W.E., Kaihatu, J.M., Petit, H.A.H., Booij, N., Holthuijsen, L.H., 2002. Diffusion reduction in an arbitrary scale third generation wind wave model. Ocean Eng. 29, 1357–1390.

Rogers, W.E., Hwang, P.A., Wang, D.W., 2003. Investigation of wave growth and decay in the SWAN model: three regional-scale applications. J. Phys. Oceanogr. 33, 366–389.

Tolman, H.L., 1991. A third-generation model for wind waves on slowly varying, unsteady and inhomogeneous depths and currents. J. Phys. Oceanogr. 21, 782–797.

Tolman, H.L., 1992. Effects of numerics on the physics in a third-generation wind-wave model. J. Phys. Oceanogr. 22, 1095–1111.

Tolman, H.L., 2002. Limiters in third-generation wind wave models. Global Atmos. Ocean Syst. 8, 67–83.

WAMDI Group, 1988. The WAM model—a third generation ocean wave prediction model. J. Phys. Oceanogr. 18, 1775–1810.

Wesseling, P., 1992. An Introduction to Multigrid Methods. John Wiley and Sons, Chichester.

Young, I.R., Verhagen, L.A., 1996. The growth of fetch limited waves in water of finite depth: Part 2. Spectral evolution. Coastal Eng. 29, 79–99.

Zijlema, M., Wesseling, P., 1998. Higher-order flux-limiting schemes for the finite volume computation of incompressible flow. Int. J. Comput. Fluid Dyn. 9, 89–109.